JACS
JOURNAL OF THE AMERICAN CHEMICAL SOCIETY

Perspective

pubs.acs.org/JACS

Charge Transfer Excitons at van der Waals Interfaces

Xiaoyang Zhu,* Nicholas R. Monahan, Zizhou Gong, Haiming Zhu, Kristopher W. Williams, and Cory A. Nelson

Department of Chemistry, Columbia University, New York, New York 10027, United States

ABSTRACT: The van der Waals interfaces of molecular donor/acceptor or graphene-like two-dimensional (2D) semiconductors are central to concepts and emerging technologies of light-electricity interconversion. Examples include, among others, solar cells, photodetectors, and light emitting diodes. A salient feature in both types of van der Waals interfaces is the poorly screened Coulomb potential that can give rise to bound electron−hole pairs across the interface, i.e., charge transfer (CT) or interlayer excitons. Here we address common features of CT excitons at both types of interfaces. We emphasize the competition between localization and delocalization in ensuring efficient charge separation. At the molecular donor/acceptor interface, electronic delocalization in real space can dictate charge carrier separation. In contrast, at the 2D semiconductor heterojunction, delocalization in momentum space due to strong exciton binding may assist in parallel momentum conservation in CT exciton formation.

There has been growing interest in molecular and quantum-confined semiconductors for light-electric interconversion, thanks to the perceived advantages of improved efficiencies, low cost, and, more interestingly, novel physics in reduced dimensions. Here we focus on two types of material interfaces for optoelectronics: (1) molecular donor/acceptor (D/A) interfaces and (2) heterojunctions of two-dimensional (2D) semiconductors, such as transition-metal dichalcogenides (TMDCs). The most critical action of light-electric interconversion occurs at these van der Waals interfaces. In both systems, dissociation of an exciton created in one material to an electron−hole pair across the material interface does not necessarily result in free carriers. Due to the low dielectric constants of molecular materials or the 2D geometry of TMDC interfaces, the Coulomb potential is poorly screened; this leads to a tightly bound electron−hole pair called a charge transfer (CT) or an interlayer exciton across the interface. The Coulomb potential is expected to be an order of magnitude higher than thermal energy at room temperature.[1−3]

A longstanding puzzle in research on donor-/acceptor-based organic photovoltaics (OPVs) is how the electron−hole pair can overcome the interfacial Coulomb potential, leading to efficient charge separation, with internal quantum efficiency as high as 100%.[4−6] A consensus arising from a large number of recent studies, both experimental[7−11] and theoretical,[12−14] is the critical role of electronic delocalization in the initial formation of a long-distance electron−hole pair, thus effectively bypassing the Coulomb trap. Such electronic delocalization, resulting from local crystallinity in molecular solids or extensive one-dimensional (1D) conjugation in rigid polymers, seems to be a hallmark of efficient OPV systems.

Recently, the van der Waals interfaces of graphene-like semiconductor crystals, such as TMDCs, are emerging as excellent models for 2D physics and for potential applications in optoelectronics.[15] Initial experiments on TMDC heterojunctions have clearly shown the efficient dissociation of an exciton created in one monolayer to form CT exciton across the interface.[16−19] Here, delocalization occurs in the plane of the 2D material, not perpendicular to the interface. In a delocalized 2D semiconductor, the large electronic band widths impart Mott−Wannier character to an exciton, which can be viewed as an electron wavepacket near the conduction band minimum (CBM) interacting with a hole wavepacket near the valence band maximum (VBM). This means that the parallel momentum vector, $\mathbf{k}_{\parallel}$, may remain a good quantum number. Since $\mathbf{k}_{\parallel}$ of an electron (hole) near the CBM (VBM) in one TMDC monolayer seldomly matches that near the CBM (VBM) in another TMDC across the heterjunction, an intriguing puzzle is how $\mathbf{k}_{\parallel}$ is conserved in interfacial charge transfer and CT exciton formation. Localization resulting from the tightly bound exciton may be a key element in ensuing parallel momentum conservation. In addition, the breaking of inversion symmetry results in an interesting interplay in the spin degrees of freedom, including electron spin, layer pseudospin, and valley pseudospins.[20,21] The valley pseudospins can be selectively excited by circularly polarized light in TMDCs, but how spin angular momentum is conserved in interlayer exciton formation/decay is an open question.

Our central thesis is that solving these puzzles requires understanding the competition between localization and delocalization. At the molecular donor/acceptor interface with a predominantly localized electronic energy landscape, it is delocalization in real space which provides the driving force for an electron−hole pair to escape the interfacial Coulomb trap. In contrast, at the TMDC interface, localization due to strong exciton binding may provide the necessary delocalization in momentum space to bring about parallel momentum conservation in interfacial CT.

LOCALIZATION AND MOMENTUM CONSERVATION IN CT AT TMDC HETEROJUNCTIONS

Following the spectacular success of graphene, graphene-like 2D semiconductors, such as TMDCs, are emerging as excellent playgrounds for 2D physics and for potential applications in

Received: March 25, 2015
Published: May 22, 2015

DOI: 10.1021/jacs.5b03141
J. Am. Chem. Soc. 2015, 137, 8313−8320

electronics and optoelectronics.[22−24] An exciting prospect is the possibility of stacking these 2D monolayers into van der Waals heterostructures.[15] These 2D heterojunctions may be grown epitaxially via chemical vapor deposition (CVD)[17] or, more generally, formed artificially via mechanical stacking.[25] In such a TMDC heterojunction, the intralayer interaction is determined by covalent bonds, while interlayer interaction is by the weaker van der Waals force. These heterojunctions may be potentially formed on large scales from roll-to-roll processing for future applications.

The 2D heterojunctions take textbook examples of interfacial physics to the limit of nanometer thickness. Figure 1 shows

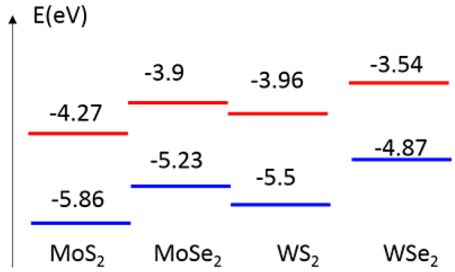

Figure 1. Band alignment of four monolayer TMDCs from ref 24. CBM: red; VBM: blue. The energy scale is the single particle energy referenced to the vacuum level.

band alignment of four TMDC monolayers.[26] The stacking of two of these TMDC layers leads to a type-II heterostructure which functions similarly as that of a p−n junction in a photovoltaic cell or photodetector. An electron−hole pair photoexcited in one material can dissociate across the 2D semiconductor interface and, eventually, leading to photocurrent generation (via contacting electrodes, such as graphene).[19] However, the primary products of interfacial charge separation are not expected to be a free electron and a free hole, but rather a tightly bound CT exciton. This is because the 2D geometry results in poor screening of the electron−hole Coulomb potential.

We show in Figure 2 results from numerical simulation of CT excitons across the model WSe_2/MoS_2 heterojunction. The MoS_2/WSe_2 bilayer is approximated as a single dielectric slab 1.37 nm in thickness, which is the sum of the van der Waals thickness of MoS_2 (0.65 nm)[27] and that of WSe_2 (0.72 nm).[28] The dielectric slab, sandwiched between vacuum, is represented by in-plane dielectric constant of $\bar{\varepsilon} = 15.1$, which is the average of those of MoS_2 ($\varepsilon = 14.5$) and WSe_2 ($\varepsilon = 15.7$).[29,30] Using a field method described by Smythe[31] and extended by Sritharan,[32] we obtain the potential experienced by an electron at (ρ, z) due to the presence of a hole at $(0, z_0)$ as

$$V(\rho) = -\frac{e^2}{4\pi\varepsilon_0\bar{\varepsilon}}\left\{\frac{(\bar{\varepsilon}-1)(\bar{\varepsilon}+1)}{\beta_P}\left[\sum_{n=0}^{\infty}\frac{(\beta_N/\beta_P)^n}{\sqrt{(z-z_0-2a+2nc)^2+\rho^2}} + \sum_{n=0}^{\infty}\frac{(\beta_N/\beta_P)^n}{\sqrt{(z-z_0+2b+2nc)^2+\rho^2}}\right] + \frac{2(\bar{\varepsilon}-1)^2}{\beta_P}\sum_{n=0}^{\infty}\frac{(\beta_N/\beta_P)^n}{\sqrt{(z-z_0+2c+2nc)^2+\rho^2}} + \frac{1}{\sqrt{(z-z_0)^2+\rho^2}}\right\} \quad (1)$$

where $\beta_N = (\bar{\varepsilon}-1)^2$ and $\beta_P = (\bar{\varepsilon}+1)^2$. The electron and the hole are confined to the center of the MoS_2 and WSe_2 monolayer, respectively, with a distance of 0.685 nm apart.

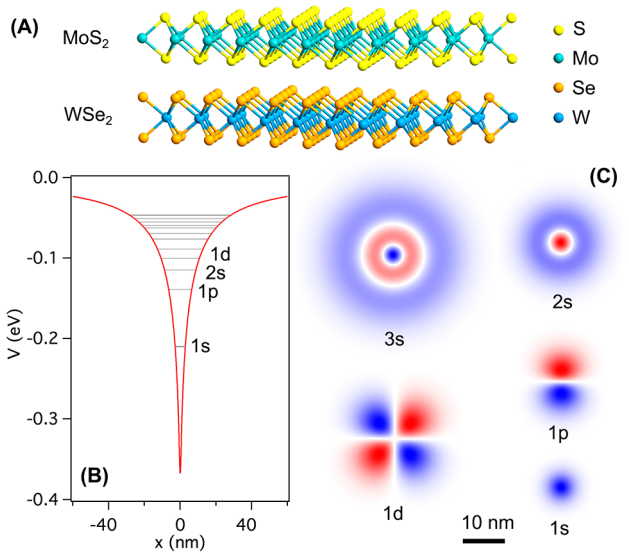

Figure 2. (A) Atomistic model of a 2D heterojunction between MoS_2 and WSe_2. (B) Model Coulomb potential as a function of in-plane radius for an electron−hole pair across the MoS_2/WSe_2 van der Waals interface. Also shown on the potential are a few eigen energies. (C) Wave functions of five CT excitons (red/blue: negative/positive).

Fixing the electron−hole separation in this manner reduces the problem from three to two dimensions. In such a 2D approximation, the freedom of motion in the surface normal direction (z) is neglected and the excitonic quasi-particle is confined to the 2D plane. We incorporate the above potential into an effective mass Hamiltonian and solve it on a 200 × 200 nm plane using the finite element method in the COMSOL Mutiphysics software. The effective mass (μ) of the excitonic quasi particle is obtained from $1/\mu = 1/m_{e^*} + 1/m_{h^*}$, where m_{e^*} and m_{h^*} are the effective masses of the MoS_2 conduction band and the WSe_2 valence band, respectively.[33,34] Solution to the Schrödinger equation yields the eigenvalues (gray lines in Figure 2B) and selected eigenfunctions (Figure 2C). We obtain a 1s CT exciton binding energy of $E_{ex} = 0.21$ eV and a mean radius of $\langle\rho_{CT_{1s}}\rangle = 2.1$ nm. For the MoS_2/WSe_2 heterojunction supported on a SiO_2 substrate, the increased screening reduces the exciton binding energy to $E_{ex} = 0.12$ eV and increases $\langle\rho_{CT_{1s}}\rangle$ to 2.3 nm.

The same model for the exciton in a single MoS_2 monolayer gives a 1s exciton binding energy of $E_{ex} = 0.50$ eV, which is close to the experimental value of $E_{ex} = 0.55$ eV reported by Ugeda et al.[35] and theoretical value of $E_{ex} = 0.54$ eV by Berkelbach et al.[30] The exciton binding energy decreases to $E_{ex} = 0.28$ eV for a MoS_2 monolayer supported on a SiO_2 substrate due to increased screen in half space. Our model also gives $\langle\rho_{1S}\rangle = 1.0$ and 1.2 nm for a suspended MoS_2 monolayer (in vacuum) and the monolayer supported on SiO_2, respectively. Since the mean radius is only ∼3 times the unit cell dimensions, the excitons in 2D TMDCs belong to the marginal case in between a typical Mott−Wannier exciton and a Frenkel exciton,[36] while that of the CT exciton is 6−7 times the unit cell dimension and is better represented by a Mott−Wannier exciton.

Several reports appeared recently on CT at TMDC interfaces formed from either the transfer stacking or CVD growth of one TMDC monolayer on another. A consensus from all reports is that, when one or both TMDC monolayers are photoexcited,

DOI: 10.1021/jacs.5b03141
J. Am. Chem. Soc. 2015, 137, 8313−8320

interfacial CT occurs on ultrafast time scales. The most common evidence is the efficient quenching of photoluminescence (PL) from intralayer excitons when a TMDC heterojunction is formed. Figure 3 shows results from our lab

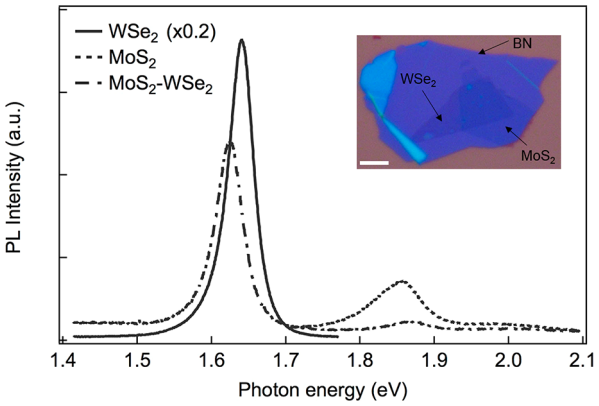

Figure 3. PL spectra from (i) WSe_2 monolayer region (solid, ×0.2), (ii) MoS_2 monolayer region (dashed), and (iii) MoS_2/WSe_2 bilayer region (dot-dashed) of a heterojunction sample capped with BN multilayers (inset). We prepared a WSe_2 monolayer flake on a SiO_2/Si substrate via exfoliation. We used a poly-propylene carbonate (PPC) capped poly-dimethylsiloxane (PDMS) to first pick up a BN flake (~20 nm thick) and then a MoS_2 monolayer flake. The BN/MoS_2 structure is then stamped onto the target WSe_2 monolayer. We kept the substrate at 120 °C for 5 min before lifting the PDMS and then rinsed the sample in acetone to remove the PPC residue on top of the BN. The result is the van der Waals stack of $BN/MoS_2/WSe_2$ on the SiO_2/Si substrate shown in the inset (scale bar 5 μm). The as-prepared sample was annealed at 300 °C for 4 h under high vacuum (10^{-8} mbar). The PL spectra were obtained on a confocal Raman/PL microscope system (ReniShaw, inVia) with excitation at 532 nm through a 100× objective and emission collected by the same objective and detected on a CCD camera.

for a transfer-stacked heterojunction of WSe_2/MoS_2 capped by BN thin films,[37,38] as shown by the optical microscopy image in the inset. A comparison of PL spectra from the monolayer regions (dashed: WSe_2; solid: MoS_2) with that from the heterojunction region (dot-dashed) shows that PL intensity from WSe_2 or MoS_2 is decreased by 80−90% at the heterojunction. In principle, the quenching of intralayer PL could be used to quantify the interlayer CT rate. The ~1 order of magnitude decrease in PL intensity would suggest that the rate of interfacial charge (e or h) transfer should be approximately 1 order of magnitude higher than the intrinsic radiative recombination rate. This calculation is unfortunately not feasible, due to the unavoidable heterogeneity of the TMDC interface. The transfer stacking of two TMDC monolayers is expected to result in a heterogeneous interface. A large portion of interfacial area may be characterized by intimate van der Waals contact and strong electronic coupling, leading to efficient CT; a small portion of the interface may possess weak electronic coupling, due to the presence of adsorbed or trapped molecules (contaminants or ambient gases). Thus, the remaining intralayer PL for WSe_2 or MoS_2 at the heterojunction likely comes from regions of weak coupling. Indeed, transient bleaching of intralayer exciton in one TMDC monolayer from photoexitation of the other, which is sensitive only to the CT part of the dynamics, reveals ultrafast (≤100 fs) CT.[18,39]

More insight into interlayer CT excitons can come from direct spectroscopic probes, such as absorption or emission. This is very challenging because optical transition strength associated with CT states across the interface is expected to be very weak due to the indirect nature of the interfacial CT gap.[40,41] To elaborate, the conduction band of one TMDC material usually does not overlap with the valence band of another in momentum space. While there have been no experimental data on optical absorption of interlayer CT excitons, three groups presented evidence for fluorescence emission from these states that are located in the optical gaps of either TMDC monolayer.[17,42,43] Gong et al. reported interlayer CT exciton emission at the MoS_2/WS_2 heterojunction only from epitaxial CVD growth, but not from transfer stacking.[17] In contrast, Rivera et al. reported interlayer CT exciton emission from transfer stacked $MoSe_2/WSe_2$.[42] One could argue that the transfer-stacked sample of Gong et al., but not of Rivera et al., might contain significant contaminants that weakened interfacial coupling. However, it is particularly surprising that Fang et al. reported interlayer CT state emission from $MoSe_2/WSe_2$ heterojunctions, even when the two TMDC monolayers are separated by 1 or 2 layers of the wide bandgap 2D dielectric material of hexaganol BN.[43]

A surprising finding from recent studies on ultrafast CT at TMDC interfaces is the absence of strong dependence of interlayer CT rate on the relative orientation of the two TMDC monolayers.[18,19,42] For a transfer-stacked heterojunction, the relative orientation of the two TMDC monolayer lattices is not aligned in real or momentum spaces, except for unlikely events of accidental alignment. Since the CBM in each of the TMDC monolayers is located at the *K* point with high parallel momentum vector, the *K* points of the two TMDC monolayer are not expected to be located in the same momentum space.[40,41,44,45] As a result, electron transfer from one TMDC monolayer to another across an artificially stacked heterojunction is expected to be accompanied by a large momentum change. A similar argument can be applied to the VBM, which is located at the *K* point in some cases or the Γ point in others, depending on the details of bilayer coupling.[40,41] Thus, hole transfer across a heterojunction interface is also expected to be accompanied by parallel momentum change. We propose two potential mechanisms for momentum conservation in interfacial CT across monolayer TMDC heterojunctions.

The first mechanism for momentum conservation is based on the excess energy for CT at a type-II heterojunction, Figure 1. In the presence of strong electronic coupling, resonant electron (hole) transfer occurs not directly from one CBM (VBM) to another CBM (VBM). Instead, we expect electron (hole) transfer to occur from the CBM (VBM) of one TMDC monolayer to the conduction (valence) bands above (below) CBM (VBM) of the other. The excess energy available to the transferred electron (hole) allows the sampling of a broader range of $\mathbf{k}_{\parallel}$ space than what is determined by the CBM (VBM) of the stacked heterojunction.

The second mechanism for momentum conservation comes from the tightly bound nature of interlayer CT excitons. Due to the poor screening of Coulomb potential in the 2D geometry, the exciton binding energies are 1−2 orders of magnitude higher than that of a typical Mott−Wannier exciton in three-dimensional (3D) semiconductors. As a result, the exciton in each TMDC monolayer or across the interface is highly localized in real space. The dielectric model illustrated in Figure 2 yields mean radii of $\langle R \rangle$ = 0.74 and 1.1 nm for an exciton in

DOI: 10.1021/jacs.5b03141
J. Am. Chem. Soc. 2015, 137, 8313−8320

MoS_2 monolayer and across MoS_2/WSe_2 interface, respectively. The corresponding uncertainties in radii:

$$\sigma_\rho = [\langle \rho^2 \rangle - \langle \rho^2 \rangle]^{1/2} \quad (2)$$

are 0.65 and 1.3 nm for excitons in an MoS_2 monolayer and across the MoS_2/WSe_2 interface, respectively. Based on the uncertainty principle and the above uncertainty in position, we may estimate uncertainties in parallel momentum vectors as $\Delta \mathbf{k}_{\parallel} \approx 1.5$ nm^{-1} (MoS_2) and 0.8 nm^{-1} (MoS_2/WSe_2). For a unit cell dimension of 0.32 nm for MoS_2,[40] the parallel momentum vector at the zone boundary is 3.1 nm^{-1}. Thus, the momentum uncertainty resulting from excitonic localization can cover up to half of the Brillouin zone and largely satisfy the requirement of momentum conservation in interfacial CT. Further localization can come from intrinsic disorder, such as structural disorder due to the softness of the 2D lattice and electrostatic disorder from the local environment.

Note that the above mechanism for fulfilling the momentum conservation based on the exciton localization applies to transition from a localized exciton in one TMDC material to a localized CT exciton across the interface. It does not apply to the transfer of a single carrier (electron or hole), which requires strict parallel momentum conservation, as demonstrated recently by Mishchenko et al. for resonant tunneling in a graphene/boron nitride/graphene structure.[46]

Two goups reported direct detection of photocurrent in ultrathin photovoltaic cells with MoS_2/WSe_2 or MoS_2/WS_2 as the active "p−n" junction and conventional metal or graphene as contacting electrodes.[19,47] It is intriguing how an electron−hole pair can overcome the large Coulomb potential (∼0.2 eV) to yield photocurrent. One possibility is that the excess energy available to the transition from an exciton in one TMDC material to the CT exciton manifold results in hot CT excitons with lower binding energies and larger electron−hole distances than those of CT_{1s}. The hot CT excitons may easily dissociate in the presence of a built-in potential resulting from CT between the two TMDC monolayers (similar to that at a p−n junction) and/or from the workfunction difference between the two contacting electrodes, before relaxing to CT_{1s}. The propensity for the formation of an electron−hole pair with large spatial separation, which favors further charge separation and photocurrent generation, is facilitated by the excess energy for CT and lateral electronic delocalization in each TMDC monolayer. As we show below, a similar mechanism is believed to be responsible for efficient charge separation at molecular donor/acceptor interfaces.

DELOCALIZATION AND CHARGE SEPARATION AT MOLECULAR DONOR/ACCEPTOR INTERFACES

Given the known low dielectric constants of molecular materials, the electron−hole Coulomb attraction energy is estimated to be in the range of 10^2 meV,[1−3] which is approximately 1 order of magnitude higher than thermal energy at room temperature. Indeed, bound CT excitons across D/A interfaces have been observed in different experiments, such as red-shifted luminescence below the optical gaps of the donor and the acceptor in D/A blends,[48−50] direct photocurrent generation from below-gap excitations,[51,52] and the formation of transient electric field as revealed by nonlinear optical spectroscopy shown below.[7]

The presence of interfacial electric field from CT exciton formation is illustrated in Figure 4 for photoinduced CT at the molecular D/A interface between copper phthalocyanine (CuPc) and fullerene (C_{60}).[7] Here, interfacial charge separation is manifested in the transient electric field, as probed by femtosecond time-resolved second-harmonic generation (TR-SHG). The detection of transient interfacial electric field is based on four-wave mixing in which two optical fields at frequency ω mixes with the pseudo-direct current (DC) field at the interface to yield second harmonic signal at 2 ω.[53] Figure 4A shows the optical absorption spectra of CuPc and C_{60} in the planar bilayer thin film structure. The first singlet (S_1) transition of CuPc consists of the doublet at 2.00 and 1.76 eV due to Davydov splitting. For the CuPc/C_{60} bilayer, the pump photon energy of ∼1.6−2.2 eV excites the CuPc S_1 state, followed by electron transfer from the lowest unoccupied molecular orbital (LUMO) of CuPc to the LUMO of C_{60} to create a CT exciton. The CT exciton can also be excited direct at lower photon energy (∼1.3−1.6 eV), albeit with a photoexcitaiton cross section two orders of magnitude lower than that for the CuPc S_1 transition.[7] The two channels for interfacial CT exciton formation, illustrated in the inset of Figure 4A, are verified in TR-SHG measurements, Figure 4B. For initial photoexcitation of the CuPc S1 state at $h\nu$ = 1.85−2.10 eV, the TR-SHG profile can all be described by a rise time of τ_{rise} = 80 ± 20 fs (blue curve), corresponding to the ultrafast and indirect formation of interfacial CT exciton. When $h\nu$ is decreased to 1.55 eV (gray), the TR-SHG profile rises faster than those at higher photon energies and can be described essentially by an instantaneous rise with τ_{rise} = 0 ± 20 fs (red curve, convoluted with the finite laser pulse width). Thus, the

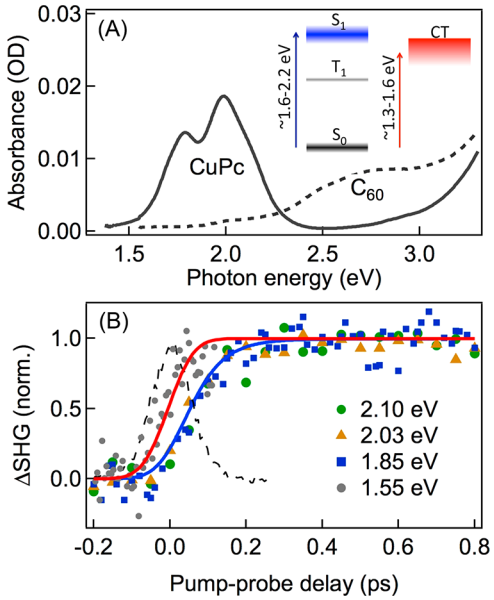

Figure 4. TR-SHG pump−probe profiles of the CuPc−fullerene interface showing indirect and direct formation of interfacial CT excitons. (A) Optical absorption spectra of CuPc (solid) and C_{60} (dashed) thin films. The inset illustrates direct optical excitation of the CuPc S_1 state (blue arrow) or the CuPc-C_{60} CT exciton state (red arrow) for the TR-SHG measurements. (B) TR-SHG spectra of 3 nm CuPc on 20 nm C_{60} excited at $h\nu$ = 2.10 (green), 2.03 (orange), 1.85 (blue), and 1.55 eV (gray). Dots are experimental data points, and solid curves are kinetic fits. The black dashed curve is pump−probe laser cross-correlation. The probe laser wavelength is 810 nm, and the SHG signal is detected at 405 nm. Modified from ref 7 with permission from Nature Publishing Group.

DOI: 10.1021/jacs.5b03141
J. Am. Chem. Soc. 2015, 137, 8313−8320

interfacial CT exciton is created directly from optical excitation at this photon energy.

Perhaps the most interesting question on charge separation at molecular D/A interfaces is the following: How does efficient separation occur at a D/A interface in the presence of tightly bound interfacial CT excitons? There are two plausible interpretations: (i) the dissociating electron–hole pair does not fall into the CT exciton trap; or (ii) the CT exciton binding energy is reduced to thermal energy when the electron–hole Coulomb potential is countered by a potential landscape in the opposite direction.

The mechanism of bypassing the CT exciton trap for efficient charge separation has gained broad support from recent experiments and computational analysis. The key to this interpretation is the presence of electronic delocalization, which leads to the ultrafast formation of a long-distance electron–hole pair across the D/A interface, thus effectively bypassing the CT exciton trap.[54] Figure 5 summarizes schematically our understanding of such a mechanism: the blue region depicts the S_1 state created by initial optical excitation. In the presence of sufficiently large electronic delocalization in the acceptor, donor, or both, we can represent the electronic energy landscape as a function of electron–hole separation (r) by the Coulomb potential (dashed curve). The Coulomb potential can be divided into two regions (green arrows): for sufficiently large r, the Coulomb potential energy is on the order of or smaller than thermal energy and the electron–hole pair can be treated as charge separated (CS) states. For smaller r where the Coulomb attraction energy is sufficiently large, the electron–hole separation is within the CT region and can collapse to the lowest CT state, i.e., a contact molecular pair, with an eventual fate of electron–hole recombination. The critical electron–hole distance (r_c) separating these two regions is essentially the so-called Coulomb capture radius in Onsager's model for ionization in the solution.[55]

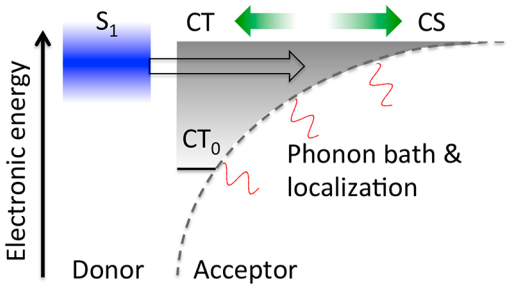

Figure 5. Schematic illustration of charge separation at a donor/acceptor interface. The singlet exciton in the donor is shown in blue. The CT excitons and CS states across the interface are in gray. The shades represent increasing DOS with energy in the CT–CS manifold defined by the Coulomb potential (dashed curve). The red curves represent electron–phonon coupling.

Since the CS and CT states depicted in Figure 5 are described by the same Coulomb potential, we have previously called the CS states "hot CT" excitons, in the spirit of Onsager's definition of a "hot" electron. The CS states have also been called nonrelaxed exciplexes, long-range geminate pairs, bound radical pairs, or polaron pairs. A misunderstanding can come from the oversimplified cartoon in Figure 5, which depicts a 1D electronic energy landscape. One should not forget that charge separation occurs in a multidimensional space, with the 3D electronic degrees of freedom intimately coupled to the phonon bath (illustrated by red wiggles on the schematic).

The 3D space for charge separation dictates that the density of states (DOS) increases rapidly with increasing electron–hole separation. This can be understood from two aspects: (1) the DOS in spherical coordinate for an isotropic medium increases with $|r|^2$; and (2) in a hydrogenic system defined by the Coulomb potential, the DOS increases with energy as DOS $\propto (BE)^{-3/2}$, where BE, the exciton binding energy, is given by the difference between the exciton energy at infinite electron–hole separation and that at r: $BE = E(\infty) - E(r)$. Such an increase in DOS with r provides an entropic driving force for charge separation.

Electron–phonon coupling can serve to localize the electron–hole pair at every stage of charge separation, leading to a self-trapped CT exciton (for small r) or e and h polarons (large r). In the latter case, localization due to electron–phonon coupling can effectively screen the electron–hole attraction potential, thus facilitates charge separation. One should also note that interfacial charge separation is a dynamic process. Electron–phonon coupling occurs on the time scale proportional to the inverse of the vibrational frequency. Only when the localization process is more or less complete should one call the electron–hole pair a polaron pair.

Photophysical studies on many D/A systems have revealed that photoexcitation of the donor can lead to charge separation across the interface on the ultrafast time scale of ~100 fs. Increasing experimental evidence now points to electronic delocalization in mediating long-range charge separation. Jailaubekov et al. directly probed CT exciton energy at the CuPc/C_{60} interface shown in Figure 4 using time-resolved two-photon photoemission (TR-2PPE) spectroscopy.[7] These authors found that ultrafast charge separation in ≤100 fs leads to the formation of long-rang and "hot" CT excitons that can relax by ~300 meV within the Coulomb potential on the time scale of ~1 ps. This conclusion is supported by Gélinas et al., who concluded, based on Stark effects from the transient electric field, that long-range charge separation up to ~4 nm occurs within 40 fs following optical excitation of the donor.[8] Falke et al. observed coherent vibrational motion in the fullerene acceptor upon photoexcitation of a conjugated polymer/fullerene blend and suggested that coherent electronic nuclear coupling plays a key role in charge delocalization and transfer.[9] Provencher et al. applied time-resolved resonance Raman spectroscopy to polymer/fullerene heterojunctions and concluded that polarons, with nearly completely relaxed nuclear coordinates, emerge within 300 fs after photoexcitation.[10] Thus, electron–phonon coupling leads to the ultrafast localization of charge carriers and nearly complete screening of the Coulomb potential on this time scale. Bernardo et al. reported a scaling of CT energy with dielectric constant in small molecule/fullerene bulk heterojunctions and suggested a threshold C_{60} crystallite size of ~4 nm in providing sufficient electronic delocalization for charge separation.[11]

A number of theoretical/computational studies have also provided support to the mechanistic picture of electronic delocalization and ultrafast charge separation. In conjunction with experiments, Jailaubekov et al. carried out nonadiabatic mixed quantum mechanics/molecular mechanics simulation on the CuPc/C_{60} system and concluded that electronic delocalization in the donor and/or acceptor, as well as nuclear fluctuation in bringing about energetic resonance, is responsible for long-distance CT.[7] Tamura and Burghardt, based on electronic

DOI: 10.1021/jacs.5b03141
J. Am. Chem. Soc. 2015, 137, 8313–8320

structure calculations and quantum dynamics simulation, suggested that electronic delocalization and excess vibrational energy in the CT manifold can promote charge separation.[12] Bittner and Silva applied an exciton lattice model to polymer/fullerene heterojunctions and suggested that resonant tunneling mediated by environmental fluctuations couples initial photoexcitation in the donor directly to CT states on <100 fs time scales.[13] Savoi et al. suggested a unique role of the nearly spherical fullerene molecule in providing a high DOS, which increases with energy; these authors showed that resonant coupling of photogenerated donor excitons to the high-energy fullerene acceptor DOS is responsible for efficient (and long distance) electron transfer, thus bypassing the CT exciton traps.[14]

The idea of hot or long-distance electron−hole pairs as responsible for photocurrent generation has also received support from experiments demonstrating the role of excess electronic energy at D/A interfaces. Such excess energy can come from excess excitation photon energy[56,57] or from additional photoexcitation which promotes localized CT excitons to more delocalized CS states in a so-called pump−push experiment.[58] Interestingly, three papers have reported efficient charge separation in OPVs even from the lowest CT excitons populated directly from below gap optical excitation.[59−61] This seems possible only if the CT exciton binding energy is much reduced to values closer to thermal energy. This scenario may arise if the Coulomb attraction is countered by a free energy landscape favoring charge separation across the D/A interface. Such a free energy gradient can come from interfacial dipoles,[62,63] structural inhomogeneity from the bulk of a donor (acceptor) to the interface,[64,65] and the presence of mixed or a hierarchy of structures between two organic materials.[66,67] In addition, the increased DOS away from the interface, as discussed earlier, provides an entropic driving force for charge carrier separation.[4,68] The presence of such free energy gradient favoring charge separation may be representative of good OPV cells.

CT EXCITONS ON ORGANIC SEMICONDUCTOR SURFACES

A Model System. An excellent model for exploring the physics of interfacial CT excitons is the CT exciton manifold on the organic semiconductor surface, first discovered in 2008 by Muntwiler et al. on the pentacene surface.[69] At such an interface, the organic semiconductor is the "donor" and the free-electron-like image potential band as the "acceptor". As shown in Figure 6A, an electron on an organic semiconductor surface with a hole in the HOMO is bound by the composite Coulomb potential of the electron-image attraction and electron−hole attraction:

$$V(\rho, z) = -\frac{\beta e^2}{16\pi\varepsilon_0}\cdot\frac{1}{z} - \frac{\gamma e^2}{4\pi\varepsilon_0}\cdot\frac{1}{\sqrt{\rho^2 + (z - z_h)^2}} \quad (3)$$

where $\beta = (\varepsilon - 1)/(\varepsilon + 1)$, $\gamma = 2/(\varepsilon + 1)$, and ε (= 5.3 for pentacene) is the dielectric constant and ε_0 is the vacuum permittivity; ρ is the lateral distance of the electron from the localized hole and z is the vertical distance of the electron from the surface; and z_h is the position of the localized hole below the surface. Figure 6B shows two cuts of the 3D potential in the XZ and XY planes; the former emphasizes the image potential (first term in eq 3) and latter the excitonic potential (second term in eq 2). Numerical solution based on the Schrödinger

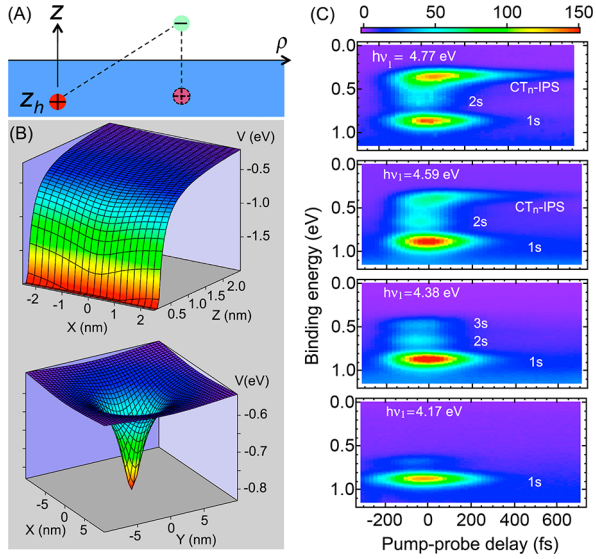

Figure 6. (A) Schematic illustration of an electron on a polarizable surface, with a localized hole located at z_h. (B) The Coulomb potential in the XZ-plane (top) and XY-plane (bottom). (C) TR-2PPE spectra with in the CT−CS manifold defined by the Coulomb potential (dashed curve). Modified from ref 70 with permission from the American Physical Society.

equation[69,70] yields a set of eigenfunctions similar to those in Figure 2, with CT exciton eigen energies converging to the image potential state (IPS), i.e., an electron bound by the image potential only and no longer interacting with the localized hole.

These CT excitons are confined to the organic semiconductor surface with high cross sections for optical excitation and ionization. Both properties permit easy detection by TR-2PPE, in which the first photon ($h\nu_1$) creates the CT exciton states and the second photon ($h\nu_2$) ionizes each CT exciton for electron detection with exquisite energy resolution. Figure 5C shows as examples TR-2PPE spectra with different excitation photon energies (from bottom to top: $h\nu_1$ = 4.17, 4.38, 4.59, and 4.77 eV) and ionization photon energies $h\nu_2 = 1/3h\nu_1$.[70] The binding energy is given by the difference between the vacuum level and the CT exciton energy. For the lowest $h\nu_1$, excitation within the CT manifold is limited to the 1s CT exciton state. With increasing $h\nu_1$, we see the population of 2s, 3s, and a high density and unresolved series of CT exciton states converging to the IPS.

As the quantum number (and energy) increases, the CT excitons become increasingly delocalized and eventually merge into the IPS, which is completely delocalized in the surface plane. Indeed, we have recently observed that high-lying CT exciton states initially populated by optical excitation can spontaneously delocalize (and gain energy) in <100 fs, a process facilitated by entropic gain due to the higher DOS closer to the asymptotic IPS limit.[71] This is analogous to the delocalization-mediated charge separation at molecular D/A interfaces, as discussed in the previous section.

SUMMARIES AND PERSPECTIVES

We show in this perspective the common physics of CT excitons formed in the poorly screened Coulomb potential at the van der Waals interface of either 2D TMDCs or molecular donors/acceptors. In both cases, the presence of electronic delocalization may favor the formation of long-distance CS states. Understanding the competition between localization and

DOI: 10.1021/jacs.5b03141
J. Am. Chem. Soc. 2015, 137, 8313−8320

delocalization is key to formulating a mechanistic picture in these systems. At molecular D/A interfaces, electronic delocalization can come from local crystallinity and extensive π-conjugation. In the case of 2D TMDC heterojunctions, we propose that momentum conservation in interfacial CT may be satisfied by the available excess energy which allows the sampling of a large momentum space and by momentum delocalization of both intra- and interlayer excitons resulting from the large exciton binding energy (and thus tight spatial localization).

A major hurdle to understanding interfacial CT excitons is the lack of experimental tools that can specifically probe these states. The strongest evidence has come from fluorescence below the optical gap of either material on two sides of the interface.[17,42,48−50] One needs to be cautious, as below-gap fluorescence may also come by trap states that are energy sinks in the system. Ideally, one would like to directly obtain optical absorption spectra from the interfacial CT excitons, but their low transition dipole moments and overwhelming interference from bulk material make the approach exceptionally challenging.[61] An exciting prospect is the possibility of applying interface specific nonlinear optical spectroscopies, such as second-harmonic generation (SHG), to map out the CT resonance.[72] Another approach is to directly probe the interfacial CT excitons by ionization in TR-2PPE, as illustrated for CT excitons on organic semiconductor surfaces (Figure 6). The TR-2PPE technique is applicable to real heterojunctions when the thickness of the top layer is not much more than the electron escape depth.[7] In this regard, a van der Waals heterojunciton of the atomically thin TMDCs represents an ideal sample for TR-2PPE probe. For a conduction band electron located at high momentum points (e.g., *K*-point), parallel momentum conservation in the photoemission process necessitates the use of ionization photon energy much higher than what is available from conventional laser sources.[73] Fortunately, tabletop extreme ultraviolet lasers based on high harmonic generation are becoming available.[74] These powerful experimental capabilities, along with improved sample preparation and theoretical/computational treatments, are essential to the advancement in our understanding of interfacial CT excitons.

AUTHOR INFORMATION

Corresponding Author

*xyzhu@columbia.edu

Notes

The authors declare no competing financial interest.

ACKNOWLEDGMENTS

This work was supported by the US National Science Foundation grant DMR 1321405 for the work on organic donor/acceptor interfaces and grant DMR 1420634 (Materials Research Science and Engineering Center) for the work on 2D TMDC interfaces. X.Y.Z. thanks T. F. Heinz for fruitful discussions. Z.G. thanks J. Hone, Y. D. Kim, and F. Ye for help with sample preparation used in Figure 3.

REFERENCES

(1) Zhu, X.-Y.; Yang, Q.; Muntwiler, M. *Acc. Chem. Res.* **2009**, *42*, 1779.

(2) Veldman, D.; Meskers, S. C.; Janssen, R. A. *Adv. Funct. Mater.* **2009**, *19*, 1939.

(3) Gélinas, S.; Paré-Labrosse, O.; Brosseau, C. N.; Albert-Seifried, S.; McNeill, C. R.; Kirov, K.; Howard, I. A.; Leonelli, R.; Friend, R. H.; Silva, C. *J. Phys. Chem. C* **2011**, *115*, 7114.

(4) Clarke, T. M.; Durrant, J. R. *Chem. Rev.* **2010**, *110*, 6736.

(5) Brédas, J. L.; Norton, J. E.; Cornil, J.; Coropceanu, V. *Acc. Chem. Res.* **2009**, *42*, 1691.

(6) Zhu, X.-Y.; Kahn, A. *MRS Bull.* **2010**, *35*, 443.

(7) Jailaubekov, A.; Willard, A. P.; Tritsch, J.; Chan, W.-L.; Sai, N.; Kaake, L.; Gearba, R. I.; Leung, K.; Rossky, P. J.; Zhu, X.-Y. *Nat. Mater.* **2013**, *12*, 66.

(8) Gélinas, S.; Rao, A.; Kumar, A.; Smith, S. L.; Chin, A. W.; Clark, J.; van der Poll, T. S.; Bazan, G. C.; Friend, R. H. *Science* **2014**, *343*, 512.

(9) Falke, S. M.; Rozzi, C. A.; Brida, D.; Maiuri, M.; Amato, M.; Sommer, E.; De Sio, A.; Rubio, A.; Cerullo, G.; Molinari, E.; Lienau, C. *Science* **2014**, *344*, 1001.

(10) Provencher, F.; Bérubé, N.; Parker, A. W.; Greetham, G. M.; Towrie, M.; Hellmann, C.; Côté, M.; Stingelin, N.; Silva, C.; Hayes, S. C. *Na. Commun.* **2014**, *5*, 4288.

(11) Bernardo, B.; Cheyns, D.; Verreet, B.; Schaller, R. D.; Rand, B. P.; Giebink, N. C. *Nat. Commun.* **2014**, *5*, 3245.

(12) Tamura, H.; Burghardt, I. *J. Am. Chem. Soc.* **2013**, *135*, 16364.

(13) Bittner, E. R.; Silva, C. *Nat. Commun.* **2014**, *5*, 3119.

(14) Savoie, B. M.; Rao, A.; Bakulin, A. A.; Gelinas, S.; Movaghar, B.; Friend, R. H.; Marks, T. J.; Ratner, M. A. *J. Am. Chem. Soc.* **2014**, *136*, 2876.

(15) Geim, A. K.; Grigorieva, I. V. *Nature* **2013**, *499*, 419.

(16) Britnell, L.; Ribeiro, R. M.; Eckmann, A.; Jalil, R.; Belle, B. D.; Mishchenko, A.; Kim, Y.-J.; Gorbachev, R. V.; Georgiou, T.; Morozov, S. V.; Grigorenko, A. N.; Geim, A. K.; Casiraghi, C.; Castro Neto, A. H.; Novoselov, K. S. *Science* **2013**, *340*, 1311.

(17) Gong, Y.; Lin, J.; Wang, X.; Shi, G.; Lei, S.; Lin, Z.; Zou, X.; Ye, G.; Vajtai, R.; Yakobson, B. I.; Terrones, H.; Terrones, M.; Tay, B. K.; Lou, J.; Pantelides, S. T.; Liu, Z.; Zhou, W.; Ajayan, P. M. *Nat. Mater.* **2014**, *13*, 1135.

(18) Hong, X.; Kim, J.; Shi, S.-F.; Zhang, Y.; Jin, C.; Sun, Y.; Tongay, S.; Wu, J.; Zhang, Y.; Wang, F. *Nat. Nanotechnol.* **2014**, *9*, 682.

(19) Lee, C. H.; Lee, G. H.; van der Zande, A. M.; Chen, W.; Li, Y.; Han, M.; Cui, X.; Arefe, G.; Nuckolls, C.; Heinz, T. F.; Guo, J.; Hone, J.; Kim, P. *Nat. Nanotechnol.* **2014**, *9*, 676.

(20) Xu, X.; Yao, Y.; Xiao, D.; Heinz, T. F. *Nat. Phys.* **2014**, *10*, 343.

(21) Riley, J. M.; Mazzola, F.; Dendzik, M.; Michiardi, M.; Takayama, T.; Bawden, L.; Granerød, C.; Leandersson, M.; Balasubramanian, T.; Hoesch, M.; Kim, T. K.; Takagi, H.; Meevasana, W.; Hofmann, Ph.; Bahramy, M. S.; Wells, J. W.; King, P. D. C. *Nat. Phys.* **2014**, *10*, 835.

(22) Mak, K. F.; Lee, C.; Hone, J.; Shan, J.; Heinz, T. F. *Phys. Rev. Lett.* **2010**, *105*, 136805.

(23) Splendiani, A.; Sun, L.; Zhang, Y.; Li, T.; Kim, J.; Chim, C. Y.; Galli, G.; Wang, F. *Nano Lett.* **2010**, *10*, 1271.

(24) Lembke, D.; Bertolazzi, S.; Kis, A. *Acc. Chem. Res.* **2015**, *48*, 100.

(25) Dean, C. R.; Young, A. F.; Meric, I.; Lee, C.; Wang, L.; Sorgenfrei, S.; Watanabe, T.; Taniguchi, T.; Kim, P.; Shepard, K. L.; Hone, J. *Nat. Nanotechnol.* **2010**, *5*, 722.

(26) Gong, C.; Zhang, H.; Wang, W.; Colombo, L.; Wallace, R. M.; Cho, K. *Appl. Phys. Lett.* **2013**, *103*, 053513.

(27) Radisavljevic, B.; Radenovic, A.; Brivio, J.; Giacometti, V.; Kis, A. *Nat. Nanotechnol.* **2011**, *6*, 147.

(28) Fang, H.; Chuang, S.; Chang, T. C.; Takei, K.; Takahashi, T.; Javey, A. *Nano Lett.* **2012**, *12*, 3788.

(29) Ramasubramaniam, A. *Phys. Rev. B* **2012**, *86*, 115409.

(30) Berkelbach, T. C.; Hybertsen, M. S.; Reichman, D. R. *Phys. Rev. B* **2013**, *88*, 045318.

(31) Smythe, W. R. *Static and Dynamic Electricity*, 2nd ed.; McGraw-Hill: New York, 1950; pp 182−184.

(32) Sritharan, S. arXiv:1312.7392. 2013, arXiv.org e-Print archive. http://arxiv.org/abs/1312.7392.

(33) Thilagam, A. *J. Appl. Phys.* **2014**, *116*, 053523.

(34) Cheiwchanchamnangij, T.; Lambrecht, W. R. *Phys. Rev. B* **2012**, *85*, 205302.

DOI: 10.1021/jacs.5b03141
J. Am. Chem. Soc. 2015, 137, 8313−8320

(35) Ugeda, M. M.; Bradley, A. J.; Shi, S. F.; Felipe, H.; Zhang, Y.; Qiu, D. Y.; Ruan, W.; Mo, S.-S.; Hussain, Z.; Shen, Z.-X.; Wang, F.; Louie, S. F.; Crommie, M. F. *Nat. Mater.* **2014**, *13*, 1091.
(36) Klingshirn, C. *Semiconductor Optics*, 2nd ed.; Springer: Berlin, 2007.
(37) Lee, C.-H.; Lee, G.-H.; van der Zande, A. M.; Chen, W.; Li, Y.; Han, M.; Cui, X.; Arefe, G.; Nuckolls, C.; Heinz, T. F.; Guo, J.; Hone, J.; Kim, P. *Nat. Nanotechnol.* **2014**, *9*, 676.
(38) Wang, L.; Meric, I.; Huang, P. Y.; Gao, Q.; Gao, Y.; Tran, H.; Taniguchi, T.; Watanabe, K.; Campos, L. M.; Muller, D. A.; Guo, J.; Kim, P.; Hone, J.; Shepard, K. L.; Dean, C. R. *Science* **2013**, *342*, 614.
(39) Ceballos, F.; Bellus, M. Z.; Chiu, H. Y.; Zhao, H. *ACS Nano* **2014**, *8*, 12717.
(40) Kośmider, K.; Fernández-Rossier, J. *Phys. Rev. B* **2013**, *87*, 075451.
(41) Komsa, H. P.; Krasheninnikov, A. V. *Phys. Rev. B* **2013**, *88*, 085318.
(42) Rivera, P.; Gong, Z.; Jones, A. M.; Chu, R.-L.; Yan, J.; Mandrus, D. G.; Zhang, C.; Cobden, D.; Yao, W.; Xu, X. *Nat. Commun.* **2015**, *6*, 6242.
(43) Fang, H.; Battaglia, C.; Carraro, C.; Nemsak, S.; Ozdol, B.; Kang, J. S.; Bechtel, H. A.; Desai, S. B.; Kronast, F.; Unal, A. A.; Conti, G.; Conlon, C.; Palsson, G. K.; Martin, M. C.; Minor, A. M.; Fadley, C. S.; Yablonovitch, E.; Maboudian, R.; Javey, A. *Proc. Natl. Acad. Sci. U.S.A.* **2014**, *111*, 6198.
(44) Terrones, H.; López-Urías, F.; Terrones, M. *Sci. Rep.* **2013**, *3*, 1549.
(45) He, J.; Hummer, K.; Franchini, C. *Phys. Rev. B* **2014**, *89*, 075409.
(46) Mishchenko, A.; Tu, J. S.; Cao, Y.; Gorbachev, R. V.; Wallbank, J. R.; Greenaway, M. T.; Morozov, S. V.; Zhu, M. J.; Wong, S. L.; Withers, F.; Woods, C. R.; Kim, Y.-J.; Watanabe, T.; Taniguchi, T.; Vdovin, E. E.; Makarovsky, O.; Fromhold, T. M.; Falko, V. I.; Geim, A. K.; Eaves, L.; Novoselov, K. S. *Nat. Nanotechnol.* **2014**, *9*, 808.
(47) Bernardi, M.; Palummo, M.; Grossman, J. C. *Nano Lett.* **2013**, *13*, 3664.
(48) Morteani, A. C.; Sreearunothai, P.; Hertz, L. M.; Friend, R. H.; Silva, C. *Phys. Rev. Lett.* **2004**, *92*, 247402 ().
(49) Tvingstedt, K.; Vandewal, K.; Gadisa, A.; Zhang, F.; Manca, J.; Inganas, O. *J. Am. Chem. Soc.* **2009**, *131*, 11819.
(50) Loi, M. A.; Toffanin, S.; Muccini, M.; Forster, M.; Scherf, U.; Scharber, M. *Adv. Funct. Mater.* **2007**, *17*, 2111.
(51) Vandewal, K.; Gadisa, A.; Oosterbaan, W. D.; Bertho, S.; Banishoeib, F.; Van Severen, I.; Lutsen, L.; Cleij, T. J.; Vanderzande, D.; Manca, J. V. *Adv. Funct. Mater.* **2008**, *18*, 2064.
(52) Drori, T.; Sheng, C.-X.; Ndobe, A.; Sinh, S.; Holt, J.; Vardeny, Z. V. *Phys. Rev. Lett.* **2008**, *101*, 03740.
(53) Tisdale, W. A.; Williams, K. J.; Timp, B. A.; Norris, D. J.; Aydil, E. S.; Zhu, X. Y. *Science* **2010**, *328*, 1543.
(54) Banerji, N. *J. Mater. Chem. C* **2013**, *1*, 3052.
(55) Onsager, L. *Phys. Rev.* **1938**, *54*, 554.
(56) Grancini, G.; Maiuri, M.; Fazzi, D.; Petrozza, A.; Egelhaaf, H. J.; Brida, D.; Cerullo, G.; Lanzani, G. *Nat. Mater.* **2013**, *12*, 29.
(57) Hahn, T.; Geiger, J.; Blase, X.; Duchemin, I.; Niedzialek, D.; Tscheuschner, S.; Beljonne, D.; Bässler, H.; Köhler, A. *Adv. Funct. Mater.* **2015**, *25*, 1287.
(58) Bakulin, A. A.; Rao, A.; Pavelyev, V. G.; van Loosdrecht, P. H.; Pshenichnikov, M. S.; Niedzialek, D.; Cornil, J.; Beljonne, D.; Friend, R. H. *Science* **2012**, *335*, 1340.
(59) Lee, J.; Vandewal, K.; Yost, S. R.; Bahlke, M. E.; Goris, L.; Baldo, M. A.; Manca, J. V.; Van Voorhis, T. *J. Am. Chem. Soc.* **2010**, *132*, 11878−11880.
(60) van der Hofstad, T. G.; Di Nuzzo, D.; van den Berg, M.; Janssen, R. A.; Meskers, S. C. *Adv. Energy Mater.* **2012**, *2*, 1095.
(61) Vandewal, K.; Albrecht, S.; Hoke, E. T.; Graham, K. R.; Widmer, J.; Douglas, J. D.; Schubert, M.; Mateker, W. R.; Bloking, J. T.; Burkhard, G. F.; Sellinger, A.; Fréchet, J. M. J.; Amassian, A.; Riede, M. K.; McGehee, M. D.; Neher, D.; Salleo, A. *Nat. Mater.* **2014**, *13*, 63.
(62) Ishii, H.; Sugiyama, K.; Ito, E.; Seki, K. *Adv. Mater.* **1999**, *11*, 605.
(63) Cahen, D.; Kahn, A. *Adv. Mater.* **2003**, *15*, 271.
(64) McMahon, D. P.; Cheung, D. L.; Troisi, A. *J. Phys. Chem. Lett.* **2011**, *2*, 2737.
(65) Yost, S. R.; Wang, L.-P.; Van Voorhis, T. *J. Phys. Chem. C* **2011**, *115*, 14431.
(66) Chen, W.; Xu, T.; He, F.; Wang, W.; Wang, C.; Strzalka, J.; Liu, Y.; Wen, J.; Miller, D. J.; Chen, J.; Hong, K.; Yu, L.; Darline, S. B. *Nano Lett.* **2011**, *11*, 3707.
(67) Burke, T. M.; McGehee, M. D. *Adv. Mater.* **2013**, *26*, 1923.
(68) Gregg, B. A. *J. Phys. Chem. Lett.* **2011**, *2*, 3013.
(69) Muntwiler, M.; Yang, Q.; Tisdale, W. A.; Zhu, X.-Y. *Phys. Rev. Lett.* **2008**, *101*, 196403.
(70) Yang, Q.; Muntwiler, M.; Zhu, X.-Y. *Phys. Rev. B* **2009**, *80*, 115214.
(71) Monahan, N. R.; Williams, K. W.; Kumar, B.; Nuckolls, C.; Zhu, X.-Y. *Phys. Rev. Lett.* **2015**, *115*, in press.
(72) Nelson, C. A.; Luo, J.; Jen, A.; Laghumavarapu, R. B.; Huffaker, D. L.; Zhu, X.-Y. *J. Phys. Chem. C* **2014**, *118*, 27981.
(73) Gierz, I.; Petersen, J. C.; Mitrano, M.; Cacho, C.; Turcu, I. E.; Springate, E.; Cavalleri, A. *Nat. Mater.* **2013**, *12*, 1119.
(74) Rohwer, T.; Hellmann, S.; Wiesenmayer, M.; Sohrt, C.; Stange, A.; Slomski, B.; Carr, A.; Liu, Y.; Miaja-Avila, L.; Kallane, M.; Mathias, S.; Kipp, L.; Rossnagel, K.; Bauer, M. *Nature* **2011**, *471*, 490.

DOI: 10.1021/jacs.5b03141
J. Am. Chem. Soc. 2015, 137, 8313−8320